Solar Energy
and Sustainable Development
Refereed, biannual scientific journal issued by
The Libyan Center for Solar Energy Research and Studies

Experimental Performance Optimization of LDPE/PVC Solar Chimney Power Plant: Comparative Analysis of Absorber Materials and Air Inlet Configurations

Khaled Djakhdane[1], **Benameur Afif**[2], **Mohammed Berka**[2,3*], **Rabie Naceur**[4].

[1]Engineering physics laboratory, University Ibn khaldoun BP 78, 14000 Tiaret. Algeria
[2]Faculty of Science and Technology, University Mustapha Stambouli of Mascara 29000, Algeria
[3]Department of Electronic, EPO Laboratory, University Djillali Liabes, Sidi Bel Abbès 22000, Algeria
Faculty of Sciences, Abu Bakr Belkaid University, B.P 119, Tlemcen-13000, Algeria.

E-*mail:* [3]m.barka@univ-mascara.dz

ARTICLE INFO.

Article history:
Received 14 September 2025
Received in revised form 04 December 2025
Accepted 29 November 2025
Available online 11 Febrory 2026

KEYWORDS

Absorber material optimization; Air inlet configuration; Experimental performance analysis; Renewable energy systems; Solar chimney power plant (SCPP).

ABSTRACT

This research presents a comprehensive experimental investigation examining the influence of absorber material selection and air inlet configuration on the operational efficiency of small- scale solar chimney power plants (SCPPs). A fully functional prototype system was constructed and extensively tested at the University of Tiaret, Algeria, featuring a 6-meter polyvinyl chloride (PVC) chimney tower integrated with a 3- meter diameter low- density polyethylene (LDPE) collector assembly.

The experimental methodology involved systematic monitoring of critical performance parameters, includingair velocity profiles, temperature distribution patterns, and humidity variations across multiple system configurationsover extended operational periods.

Two distinct absorber materials were evaluated: high- reflectivity aluminum and high-absorption black polymer, tested in combination with varying air inlet configurations ranging from single to quintuple inlet designs. Comprehensive data acquisition was achieved through strategically positioned LM35 temperature sensors, PCE-THA 10 thermo- hygro-anemometer measurements, and Arduino Mega microcontroller- based data logging systems.

*Corresponding author.

DOI:https://doi.org/10.51646/jsesd.v14i2.857

Experimental results demonstrate that the optimal configuration combines a black polymer absorber with a dual air inlet design, achieving superior thermal performance with maximum air temperatures reaching 78°C and chimney updraft velocities of 2.8 m/s during peak solar irradiation periods. The study reveals distinct operational phases characterized by 12-13 hours of active airflow generation, with humidity effects significantly influencing system thermodynamics, particularly in moisture-sensitive configurations. These findings provide critical design optimization data for enhancing SCPP system efficiency and establish a foundation for scaling renewable energy applications in arid and semi-arid regions where conventional energy infrastructure may be limited.

تحسين الأداء التجريبي لمحطة الطاقة الشمسية ذات المدخنة المصنوعة من البولي إيثيلين منخفض الكثافة/البولي فينيل كلوريد: تحليل مقارن لمواد الامتصاص وتكوينات مدخل الهواء

خالد جخدان، بن عامر عفيف، محمد بركة، ربيع ناصر.

ملخص: يقدم هذا البحث دراسة تجريبية شاملة تبحث في تأثير اختيار مادة الامتصاص وتكوين مدخل الهواء على الكفاءة التشغيلية لمحطات توليد الطاقة الشمسية صغيرة الحجم ذات المداخن (SCPPs). تم بناء نموذج أولي كامل الوظائف واختباره على نطاق واسع في جامعة تيارت بالجزائر، حيث يتكون من برج مدخنة من البولي فينيل كلوريد (PVC) بقطر 6 أمتار، مُدمج مع مجمع تجميعي من البولي إيثيلين منخفض الكثافة (LDPE) بقطر 3 أمتار. تضمنت المنهجية التجريبية مراقبة منهجية لمعايير الأداء الحرجة، بما في ذلك أنماط سرعة الهواء، وأنماط توزيع درجة الحرارة، وتغيرات الرطوبة عبر تكوينات متعددة للنظام على مدى فترات تشغيلية طويلة. تم تقييم مادتي امتصاص مميزتين: الألومنيوم عالي الانعكاسية والبوليمر الأسود عالي الامتصاص، واختبارهما مع تكوينات مختلفة لمدخل الهواء تتراوح بين تصميمات ذات مدخل واحد وخماسي. تم الحصول على بيانات شاملة من خلال مستشعرات درجة الحرارة LM35 الموضوعة في مواقع استراتيجية، وقياسات مقياس الحرارة والرطوبة وسرعة الرياح PCE-THA 10، وأنظمة تسجيل البيانات القائمة على متحكم Arduino Mega. تُظهر النتائج التجريبية أن التكوين الأمثل يجمع بين ماص بوليمر أسود وتصميم مدخل هواء مزدوج، مما يحقق أداءً حرارياً فائقاً مع درجات حرارة هواء قصوى تصل إلى 78 درجة مئوية وسرعات تيارات هوائية صاعدة من المدخنة تبلغ 2.8 متر/ثانية خلال فترات ذروة الإشعاع الشمسي. تكشف الدراسة عن مراحل تشغيلية مميزة تتميز بتوليد تدفق هواء نشط لمدة 12-13 ساعة، مع تأثيرات الرطوبة التي تؤثر بشكل كبير على الديناميكا الحرارية للنظام، وخاصة في التكوينات الحساسة للرطوبة. توفر هذه النتائج بيانات تحسين تصميمية مهمة لتعزيز كفاءة نظام SCPP، وترسي أساسًا لتوسيع نطاق تطبيقات الطاقة المتجددة في المناطق القاحلة وشبه القاحلة حيث قد تكون البنية التحتية للطاقة التقليدية محدودة.

الكلمات المفتاحية - تحسين مادة الامتصاص، تكوين مدخل الهواء تحليل الأداء التجريبي، أنظمة الطاقة المتجددة، محطة الطاقة الشمسية المدخنة.

1. INTRODUCTION

The global energy landscape is undergoing a profound transformation characterized by unprecedented demand growth and escalating environmental pressures. In 2024, worldwide energy consumption surged by 2.2%, nearly doubling the historical average of 1.3% observed between 2013 and 2023 [1]. This remarkable acceleration was exacerbated by extreme weather phenomena, which contributed an estimated 0.3 percentage points to the overall growth trajectory [2]. The surge reflects fundamental structural shifts in global energy utilization patterns, with developing economies expanding their industrial capabilities while developed nations grapple with increasing digitization demands. Particularly striking was the electricity sector's expansion, which reached 4.3% in 2024, the largest absolute increase ever recorded [3] outside of post-recession recovery periods. This dramatic growth stems from the rapid proliferation of energy-intensive applications, including widespread air conditioning adoption

in emerging markets, exponential expansion of digital infrastructure, proliferation of data centers, artificial intelligence computational requirements, and the accelerating electrification of transportation and industrial processes across multiple sectors.

Despite significant progress in renewable energy deployment, the global energy mix remains heavily dependent on fossil fuels, underscoring the urgent need for innovative clean energy solutions. While renewables achieved a notable 38% share of total energy supply growth in 2024, followed by natural gas (28%) and coal (15%), this progress is insufficient to meet international climate commitments [4]. The persistence of fossil fuel dominance is reflected in continued environmental degradation, with energy-related CO_2 emissions rising by 0.8% despite global climate pledges [5]. Furthermore, global energy intensity improvements remained disappointing at merely 1%, continuing the concerning slowdown observed in recent years [6]. These statistics highlight critical gaps in current renewable energy deployment strategies, particularly the need for technologies capable of operating efficiently across diverse geographical regions, varying climatic conditions, and economic development levels. The challenge is especially acute in arid and semi-arid regions of developing countries, where abundant solar resources remain largely untapped due to technological and economic barriers associated with conventional photovoltaic and concentrated solar power systems [7].

Solar Chimney Power Plants (SCPPs) emerge as a particularly promising technology for addressing these challenges, offering a unique approach to sustainable electricity generation that is exceptionally well-suited for regions with high solar irradiance and limited water resources. The fundamental operating principle of SCPPs leverages solar-induced buoyancy effects through an elegantly simple yet thermodynamically sophisticated process: solar radiation penetrates a transparent collector canopy, heating the air mass beneath and reducing its density relative to ambient conditions [8]. This density differential creates natural convective updrafts that flow through a central chimney structure, where the kinetic energy of the rising air mass drives electricity-generating turbines positioned at the chimney base or within the tower structure. The system's inherent advantages include minimal water consumption, low maintenance requirements, use of readily available construction materials [9], and the ability to operate continuously during daylight hours without complex tracking systems or high-temperature components. Unlike photovoltaic systems that suffer performance degradation in high-temperature environments [10], SCPPs actually benefit from elevated ambient temperatures, making them ideally suited for desert and semi-desert regions where conventional solar technologies face operational challenges [11].

The conceptual foundation of SCPP technology traces its intellectual origins to visionary early 20th-century innovations that recognized the untapped potential of atmospheric convection for power generation. The earliest documented proposal emerged from Isidoro Cabanyes in Spain (1903) [12], who conceptualized harnessing solar-heated air currents for mechanical work, followed by Hanns G*ü*nther's more detailed theoretical framework developed in Germany (1931) [13], which provided mathematical foundations for combining greenhouse and chimney effects in power generation applications [14]. These pioneering concepts remained largely theoretical until the late 20th century [15], when advancing materials science and engineering capabilities enabled practical implementation. The technology's technical viability was conclusively demonstrated through the landmark Manzanares experimental plant in Spain (1982–1989), a groundbreaking project that represented the first large-scale validation of SCPP principles. This ambitious prototype featured impressive dimensions, including a 244-meter-diameter collector area and a 194.6-meter-high concrete chimney, successfully

generating up to 50 kW of peak electrical power while operating continuously for seven years [16-18]. The Manzanares project provided crucial empirical data that validated theoretical predictions and demonstrated the technology's potential for commercial-scale deployment.
Building upon the Manzanares foundation, subsequent research has progressively advanced the understanding of SCPP thermodynamics, fluid mechanics, and design optimization through increasingly sophisticated experimental and computational investigations. In [19], Pasumarthi and Sherif have conducted pioneering validation studies using smaller-scale experimental systems in Florida, USA, successfully correlating theoretical heat transfer models with empirical performance data and establishing important scaling relationships for collector-to-chimney area ratios. Authors in [20] have contributed significant insights into transient thermal behavior, documenting critical operational phenomena including temperature inversions during post-sunrise periods and achieving collector-to-ambient temperature differentials reaching 24.1°C under optimal conditions, while identifying the importance of thermal mass effects on system stability. Recent advances have focused on innovative design modifications and hybrid system integration, with parametric optimization studies investigating flow variations in semi-elliptical collector curvatures to enhance energy generation while minimizing resource utilization [21]. Glass-covered collector configurations have demonstrated remarkable improvements, increasing air outlet temperature by 16.4°C and air flow rate by 34%, with thermal efficiency enhanced from 10.3% to 14.6% [22].

Experimental investigations with divergent chimney designs and optimized height parameters have shown significant power output enhancements through systematic variation of collector height, radius, and chimney dimensions [23]. The integration of thermal storage systems has gained considerable attention, with phase change material (PCM) integration studies addressing performance limitations and reliability challenges inherent to solar radiation intermittency [24]. Advanced hybrid configurations have demonstrated exceptional potential, including integrated electrolysis stations producing 13,000 kg of green hydrogen annually while generating 380,263 kWh of electrical energy [25], and coupling with water desalination plants to enhance both energy and freshwater production through excess heat recovery [26]. Innovative hybrid systems combining SCPPs with gas power plants have achieved power output increases of 554%, 208%, and 125% at different radiation flux levels through buried pipe heat recovery configurations [27]. However, despite these substantial advances in geometric optimization, hybrid integration, and thermal enhancement strategies, critical knowledge gaps persist regarding the systematic evaluation of absorber material properties, particularly the comparative performance of polymer versus metallic surfaces, and the quantitative optimization of air inlet configurations, which directly govern SCPP performance characteristics and commercial viability for deployment in diverse climatic conditions. This study addresses identified knowledge gaps through a comprehensive experimental investigation of a pilot-scale SCPP constructed and operated in Tiaret, Algeria, a location strategically selected for its exceptional solar irradiance levels and arid climatic conditions that represent ideal operational environments for SCPP deployment. Our research systematically examines two primary parameters previously under-investigated in the literature: first, absorber material selection and optimization through direct experimental comparison of high-thermal-absorption polymer materials (specifically black plastic with enhanced solar absorptivity) versus high-reflectivity metallic surfaces (aluminum with superior thermal conductivity characteristics), evaluating their relative performance in thermal energy capture efficiency, temperature distribution uniformity, and thermal stability under prolonged solar exposure. Second, we systematically evaluate 1–5 air inlet configurations to quantify their

effects on key performance parameters, including airflow velocity, temperature distribution, humidity influences, and overall thermal efficiency across diverse environmental conditions. The experimental facility incorporates a 3-meter-diameter LDPE collector optimally positioned at 30° inclination and a 6-meter-high PVC chimney with 110 cm diameter, comprehensively instrumented with precision temperature sensors (LM35), humidity monitoring systems, and velocity measurement equipment (PCE-THA 10 thermo-hygro-anemometer) strategically positioned throughout the system to enable continuous measurement of performance parameters under real operational conditions. Through systematic parametric studies conducted during optimal solar conditions (April–June period), this research aims to identify design configurations that maximize updraft velocity and thermal efficiency while minimizing system complexity and construction costs, ultimately providing actionable engineering insights and empirical data for developing scalable, cost-effective SCPP systems suitable for widespread deployment in arid regions characterized by high solar potential but limited access to conventional power infrastructure.

2. ANALYTICAL AND NUMERICAL MODELING FRAMEWORKS FOR SCPP SYSTEMS

The theoretical foundation of SCPP technology rests upon well-established thermodynamic and fluid mechanics principles, with significant research devoted to developing predictive models that relate system geometry, environmental conditions, and performance outputs. Early analytical frameworks established by Schlaich et al. [28] formulated the fundamental energy balance equations governing SCPP operation, demonstrating that power output scales proportionally with collector area, solar irradiance intensity, and the square of chimney height, while inversely relating to system pressure losses. These pioneering models utilized simplified one-dimensional approximations assuming steady-state conditions and uniform temperature distributions, providing crucial design guidelines despite inherent limitations in capturing complex three-dimensional flow phenomena and transient thermal effects [29].

Bernardes et al. significantly advanced analytical modeling capabilities by incorporating comprehensive heat transfer mechanisms, including solar radiation absorption, convective heat exchange between absorber surfaces and air masses, and radiative losses from collector surfaces, while developing coupled differential equations that simultaneously solve for temperature profiles, pressure distributions, and velocity fields throughout the collector-chimney system. Their work established critical dimensionless parameters, including the Rayleigh number characterizing buoyancy-driven flow intensity and the Nusselt number quantifying convective heat transfer efficiency, enabling systematic performance prediction across varying operational conditions and geometric configurations [30]. Subsequent refinements by Pretorius and Kröger [31] introduced more sophisticated analytical treatments incorporating turbulence effects, non-uniform solar irradiance patterns, and three-dimensional collector geometry influences, achieving improved agreement between theoretical predictions and experimental measurements from the Manzanares facility.

The evolution of computational capabilities has enabled increasingly detailed numerical simulations that overcome analytical model limitations through direct solution of governing Navier-Stokes equations, energy conservation principles, and radiation transport phenomena. Comprehensive computational fluid dynamics (CFD) investigations by Ming et al. [32] employed three-dimensional Reynolds-Averaged Navier-Stokes (RANS) turbulence modeling with k-ε closure schemes to resolve complex flow structures within SCPP systems, revealing critical insights into collector entrance effects, flow separation phenomena, and velocity profile development that significantly influence overall system efficiency. Their simulations

demonstrated that collector flow exhibits distinct radial acceleration as air moves toward the chimney base, with velocity increasing from typical inlet values of 0.5-1.0 m/s to exit velocities of 10-15 m/s in optimized configurations, while temperature fields show strong stratification with peak values occurring at approximately 0.7-0.8 of the collector radius [33]. Advanced CFD studies by Gholamalizadeh and Kim [34] incorporated sophisticated radiation models, including the discrete ordinates method (DOM) and surface-to-surface (S2S) radiation to accurately capture solar energy absorption and thermal re-radiation effects, achieving prediction accuracies within 5-8% of experimental measurements for temperature distributions and 10-15% for velocity profiles under steady-state conditions.

Transient numerical modeling has emerged as a critical research frontier, addressing SCPP performance variations throughout diurnal solar cycles and enabling optimization of thermal energy storage integration strategies. Zhou et al. [20] conducted pioneering transient simulations capturing startup phenomena, demonstrating that SCPP systems require 2-4 hours to achieve thermal equilibrium after sunrise, with temperature inversion effects occasionally occurring when absorber surface temperatures temporarily fall below ambient due to nocturnal radiative cooling. Dynamic simulations by Motsamai et al. [35] examined the influence of thermal mass on system stability and evening power generation extension, revealing that concrete or water-based thermal storage can sustain power generation for 2-6 hours beyond sunset, depending on storage capacity and solar collection efficiency during daylight periods. Recent coupled simulations integrating computational fluid dynamics with phase change material (PCM) thermal storage models have demonstrated potential for extending operational periods to nearly 24-hour continuous generation through strategic placement of encapsulated PCM modules beneath collector absorber surfaces, though experimental validation of these advanced configurations remains limited.

Despite substantial progress in analytical and numerical modeling capabilities, significant knowledge gaps persist regarding model validation against systematic experimental data, particularly for polymer-based absorber materials that exhibit different thermal response characteristics compared to traditional metallic surfaces, and for air inlet configuration optimization, where existing models rely primarily on theoretical assumptions rather than empirical validation. Most CFD studies have focused on idealized boundary conditions with uniform material properties and simplified geometric representations, while experimental investigations validating these models across diverse absorber materials, inlet configurations, and environmental conditions remain scarce [36]. Furthermore, existing analytical correlations for efficiency prediction were predominantly derived from large-scale installations (collector diameters >100 m) with limited experimental verification for small-scale prototypes (3-10 m diameter), where scaling effects, edge phenomena, and surface roughness influences may significantly deviate from theoretical predictions based on dimensional analysis. The present experimental investigation addresses these identified gaps through systematic parametric analysis of absorber material selection (polymer versus metallic surfaces) and air inlet configuration optimization (1–5 inlet arrangements), providing empirical data that enables direct validation of existing analytical and numerical models. By establishing performance correlations specifically applicable to small-scale SCPP systems (3–10 m diameter), this research bridges the knowledge gap between large-scale theoretical predictions and practical small-scale implementations. These findings offer actionable design guidelines for distributed power generation in arid regions with limited infrastructure access, where economically viable and scalable renewable energy solutions are essential for sustainable development.

3. EXPERIMENTAL SETUP

3.1. Overview and site characteristics

The experimental investigation was conducted at Ibn-Khaldoun University Park, Tiaret, Algeria (35°21'00.0"N, 1°18'47.2"E), a location strategically selected for its exceptional solar irradiance characteristics and representative arid climatic conditions. Tiaret's geographical position provides optimal solar exposure with minimal atmospheric interference, featuring average daily solar irradiation exceeding 5.5 kWh/m²/day during the experimental period (April–June). The site's elevation of approximately 1,080 meters above sea level ensures reduced atmospheric density, which enhances natural convection effects critical for SCPP operation. The experimental facility was positioned to minimize surrounding obstructions and maximize solar exposure throughout the measurement period, with prevailing wind patterns carefully considered for air inlet positioning.

3.2. Solar chimney configuration and design specifications

The prototype SCPP system was designed following established scaling principles derived from the Manzanares pilot plant, with careful attention to preserving critical dimensionless parameters that govern buoyancy-driven flow behavior and thermal conversion efficiency. The dimensional ratios were selected based on geometric similarity criteria, maintaining a chimney height-to-diameter ratio (H/D = 5.45) consistent with optimal performance ranges identified in prior CFD simulations and analytical models [8, 35], while the collector diameter-to-chimney height ratio (Dc/Hc = 0.5) was optimized to balance thermal energy collection area with structural feasibility for small-scale experimental validation. This scaling approach enables direct correlation of experimental results with theoretical predictions while specifically addressing two under-investigated parameters: absorber material thermal response characteristics (polymer versus metallic surfaces) and air inlet configuration effects (1-5 inlet arrangements), both of which significantly influence system performance but lack comprehensive empirical validation in existing literature. The prototype dimensions were further constrained by practical considerations, including material availability, instrumentation requirements for comprehensive spatial temperature mapping, and the need to achieve measurable airflow velocities (>1.5 m/s) suitable for turbine integration studies in future experimental phases.

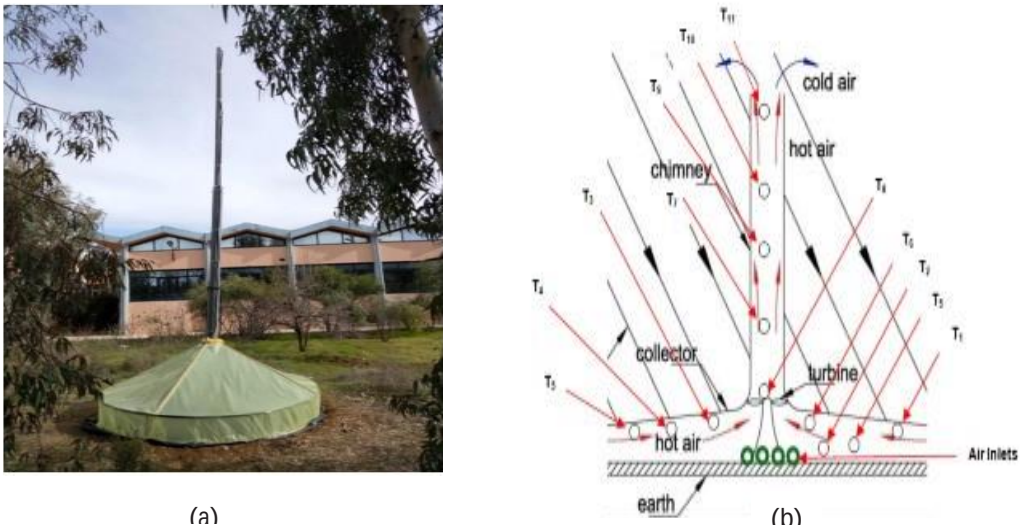

Figure 1: (a) Prototype of solar chimney (b) Temperature sensors in prototype development.

The system comprises a 3-meter-diameter circular solar collector positioned at a 30° inclination angle to maximize solar energy capture for Tiaret's latitude, providing a total collection area of 7.07 m² and featuring a low-density polyethylene (LDPE) film canopy with 200 μm thickness, 88% solar transmittance, and enhanced UV resistance for long-term outdoor exposure. The collector assembly incorporates two systematically evaluated absorber materials: high-density polyethylene black plastic with 0.95 solar absorptance and 0.88 thermal emittance for superior heat absorption characteristics, and aluminum alloy 6061-T6 with >90% solar reflectance and 167 W/(m·K) thermal conductivity for comparative analysis of reflective versus absorptive thermal strategies. The vertical chimney structure, representing the critical component for converting thermal buoyancy into directed airflow, features a 6-meter height with 1.10-meter internal diameter (height-to-diameter ratio of 5.45) constructed from polyvinyl chloride (PVC) with 3.2 mm wall thickness, selected for optimal thermal properties including 81°C glass transition temperature, 0.14 W/(m·K) thermal conductivity, and 0.91 thermal emissivity. The chimney's structural integrity is ensured through a carbon steel framework (Fe 250 grade) providing 250 MPa yield strength and economic viability with 40% lower cost than stainless steel alternatives, while maintaining service temperature capability up to 400°C. The air inlet system incorporates variable configurations (1–5 inlets) with circular geometry matching the chimney cross-sectional area, individual inlet diameters of 1.10 meters providing total inlet areas ranging from 0.95–4.75 m², strategically positioned radially around the collector perimeter opposite to prevailing wind direction. Each inlet features rounded entrance geometry with 0.05-meter radius, internal flow straightening vanes, and adjustable dampers to minimize pressure losses and ensure uniform flow distribution during systematic parametric evaluation. The complete system integration enables precise measurement of thermal and flow characteristics under varying absorber material and inlet configuration conditions, providing comprehensive data for performance optimization analysis. This configuration allows for a systematic investigation of the two critical design parameters while maintaining consistent boundary conditions and measurement accuracy throughout the experimental campaign.

3.3. Instrumentation and data acquisition system

The comprehensive instrumentation network was strategically designed to capture detailed thermal, environmental, and flow characteristics throughout the SCPP system, incorporating a distributed temperature measurement system utilizing twelve LM 35 precision temperature sensors with −55°C to +150°C measurement range, ±0.5°C accuracy, and <30-second response time, positioned at critical locations including collector inlet (2 sensors for ambient conditions), collector interior (4 sensors for spatial temperature distribution), collector outlet/chimney inlet (2 sensors for heated air temperature), chimney mid-height (2 sensors for thermal profile verification), and chimney outlet (2 sensors for exit air temperature). Environmental parameter monitoring was achieved through a PCE-THA 10 thermo-hygro-anemometer providing simultaneous measurement of temperature (−15°C to +50°C, ±0.6°C accuracy), relative humidity (5–95% RH, ±3% accuracy), and air velocity (0.4–35 m/s, ±3% reading accuracy) with integrated data logging capabilities and USB connectivity for continuous environmental characterization. The data acquisition and control system centered on an Arduino Mega microcontroller platform featuring an ATmega1280 processor with a 16 MHz crystal oscillator, 54 digital I/O pins, 16 analog input channels with 10-bit ADC resolution, and 4 UART serial ports enabling simultaneous connectivity to all sensor networks with a 1-minute sampling frequency for continuous 24-hour operation cycles. Data quality assurance was implemented through pre-experiment NIST-traceable sensor calibration, daily

cross-referencing between redundant sensors for in-situ verification, automated sensor validation with error detection algorithms, and redundant data storage systems incorporating an SD card interface with GPS time synchronization and cloud backup capabilities. The measurement protocol included systematic data filtering to exclude adverse weather conditions (precipitation, winds >15 m/s), repeatability testing under identical conditions for statistical validation, and post-experiment calibration drift assessment to ensure measurement accuracy and reliability throughout the experimental campaign. This integrated instrumentation system enables precise quantification of thermal performance, airflow characteristics, and environmental influences while maintaining high data quality standards essential for systematic parametric analysis of absorber material and air inlet configuration effects on SCPP performance.

All sensors underwent rigorous three-point calibration against NIST-traceable reference standards ($\pm$0.10C for temperature, $\pm$0.5% for humidity, $\pm$0.02 m/s for velocity) before installation, with calibration certificates documenting traceability to international standards (ISO/IEC 17025). Measurement uncertainty analysis, performed according to the Guide to the Expression of Uncertainty in Measurement (GUM), yielded combined standard uncertainties of $\pm$0.60C for temperature (accounting for sensor accuracy $\pm$0.50C, calibration uncertainty $\pm$0.10C, spatial variability $\pm$0.30C, and drift $\pm$0.20C), $\pm$3.5% for humidity measurements, and $\pm$0.15 m/s for velocity measurements under operational conditions. Each experimental configuration was tested through five complete diurnal cycles (sunrise to sunset) over consecutive clear-sky days, with data acquisition performed at 60-second intervals, yielding approximately 720 measurement points per sensor per day and a total dataset exceeding 43,000 validated data points across the 12-week experimental campaign. Repeatability testing demonstrated excellent consistency with coefficient of variation (CV) values below 4.2% for temperature measurements and below 6.8% for velocity measurements across replicate trials, while post-experiment calibration verification (conducted after campaign completion) confirmed sensor drift remained within acceptable limits (<0.30C for LM35 sensors, <2% for PCE-THA 10), ensuring data reliability throughout the extended measurement period.

3.4. Experimental methodology and test protocols

The experimental investigation employed a systematic two-phase approach designed to isolate and quantify the individual effects of absorber material selection and air inlet configuration on SCPP performance while maintaining rigorous quality control standards throughout the measurement campaign. Phase 1 focused on absorber material comparison over a 4-week (April 2024) utilizing a fixed 2-inlet configuration as a baseline, systematically evaluating black plastic versus aluminum absorber surfaces through continuous monitoring with daily performance assessment to determine optimal thermal energy capture characteristics under identical operational conditions. Phase 2 concentrated on air inlet optimization over an 8-week duration (May–June 2024) using the optimal absorber material identified from Phase 1, systematically varying inlet configurations from 1 to 5 inlets with weekly configuration changes and 3-day stabilization periods to ensure thermal equilibrium before data collection, enabling precise quantification of inlet quantity effects on airflow velocity, temperature distribution, and overall system thermal efficiency. Quality assurance protocols incorporated comprehensive sensor calibration procedures, including pre-experiment calibration against NIST-traceable references, daily in-situ cross-referencing between redundant sensors for drift detection, and post-experiment validation with calibration drift assessment and correction factor application to ensure measurement accuracy throughout the extended experimental period. Environmental controls included continuous monitoring of solar irradiance, ambient

temperature, and wind speed conditions, with systematic data filtering to exclude measurements during adverse weather conditions (precipitation, high winds >15 m/s) that could compromise measurement validity, and repeatability testing through duplicate measurements under identical conditions for statistical validation of results. The experimental protocol ensured systematic parameter isolation by maintaining consistent boundary conditions, standardized measurement procedures, and rigorous data quality control, enabling reliable assessment of absorber material and air inlet configuration effects on SCPP thermal and flow performance characteristics. This methodological approach provides comprehensive parametric analysis capabilities while ensuring high-quality, reproducible data collection suitable for engineering design optimization and scientific validation of SCPP performance enhancement strategies.

4. RESULTS, ANALYSIS AND DISCUSSION

4.1. Overview of experimental campaign

The experimental investigation was conducted over a 12-week period (April–June 2024) under optimal climatic conditions characterized by high solar irradiance (average 6.2 kWh/m²/day), low ambient humidity (15—45% RH), and minimal precipitation, providing ideal operational parameters for SCPP performance evaluation. The systematic two-phase approach enabled a comprehensive assessment of design parameters while maintaining controlled boundary conditions essential for reliable parametric analysis. All measurements were conducted during peak solar hours (08:00–18:00), representing the period of maximum solar irradiance and active system operation. Continuous 24-hour monitoring was implemented throughout the experimental campaign to comprehensively capture diurnal thermal behavior patterns, system transient responses during startup and shutdown phases, and nocturnal cooling dynamics. This extended monitoring protocol enabled complete characterization of the SCPP's thermal performance across full day-night cycles, providing critical insights into operational stability and thermal inertia effects.

4.2. Absorber material performance analysis

The comparative evaluation of absorber materials revealed fundamental differences in thermal energy capture efficiency and temperature stability characteristics, as comprehensively illustrated in Figure 2, which presents the diurnal temperature evolution profiles for both black plastic and aluminum absorber configurations measured at sensor position T3 located at the collector outlet. The black plastic absorber demonstrated markedly superior thermal performance throughout the entire measurement period, achieving sustained peak air temperatures of 78°C during optimal solar conditions (10:00–18:00 hours), representing a significant 8°C temperature advantage over the aluminum absorber's maximum recorded temperature of 70°C, corresponding to an 11.4% improvement in thermal energy capture directly attributable to the black plastic's exceptional solar absorptance coefficient ($\alpha = 0.95$) compared to aluminum's high solar reflectance ($\rho > 0.90$). Figure 2 clearly illustrates the distinct behavioral characteristics of each absorber material, with the black plastic configuration exhibiting remarkably stable and consistent temperature evolution patterns beginning with gradual temperature rise at sunrise (06:45), achieving steady-state thermal conditions within approximately 2 hours of peak solar exposure (08:30–09:00), and maintaining elevated temperatures exceeding 60°C for extended operational periods spanning 8 continuous hours (10:00–18:00). In stark contrast, the aluminum absorber demonstrated rapid initial temperature rise due to its superior thermal conductivity (167 W/m·K), as evidenced by the steeper slope in Figure 2 during early morning hours (07:00–09:00), but

subsequently exhibited pronounced temperature fluctuations and thermal instability throughout the day, particularly evident during periods of variable cloud cover and transitional solar conditions, with temperature oscillations of ±5°C compared to the black plastic's stable ±2°C variations. The temperature differential between absorber materials, clearly visible in Figure 2, remained consistently favorable for the black plastic configuration throughout the operational period, with maximum differentials reaching 10–12°C during peak solar hours (12:00–14:00) and maintaining 5–8°C advantages even during reduced solar conditions (16:00–18:00). Quantitative thermal efficiency analysis, calculated as the ratio of thermal energy gained by the air mass to incident solar radiation, revealed the black plastic absorber's superior performance with average efficiencies of 45–52% during peak solar conditions compared to 35–42% for aluminum, while Figure 2 demonstrates that the black plastic-maintained temperatures above 50°C for 10–11 hours daily compared to aluminum's 7–8-hour period above the same threshold.

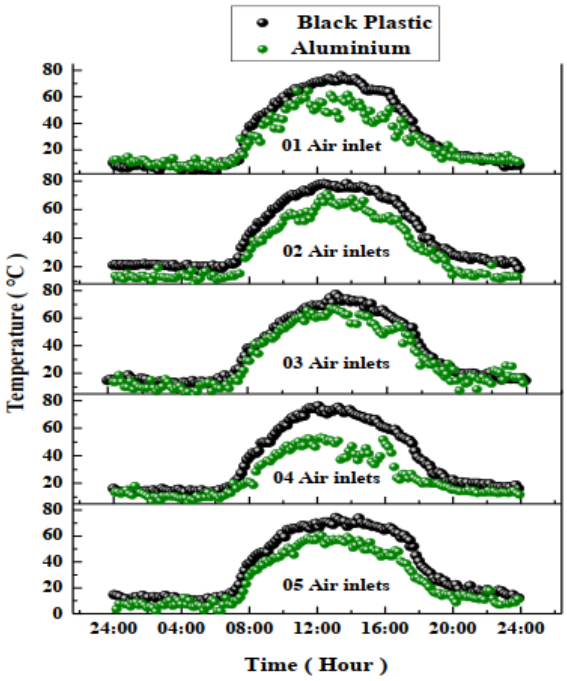

Figure 2. Comparative temperature performance: Black plastic vs. Aluminum absorbers.

The superior thermal stability exhibited by the black plastic absorber, as evidenced by the smoother temperature curves in Figure 2, results from its ability to convert absorbed solar radiation directly into thermal energy with minimal reflection losses, contrasting with aluminum's high reflectivity that reduces available thermal input despite superior thermal conductivity properties. Temperature uniformity analysis across the collector area demonstrated more consistent spatial temperature distribution with the black plastic absorber (±2.1°C standard deviation) compared to aluminum (±3.8°C), enhancing overall system efficiency by promoting uniform buoyancy forces and reducing thermal stratification effects that impede optimal airflow development. The pronounced temperature maintenance capability shown in Figure 2 for the black plastic configuration, with gradual temperature decline during evening hours (18:00–20:00) compared to aluminum's rapid temperature drop, indicates enhanced thermal mass effects and sustained energy release characteristics crucial for extended operational periods. This comprehensive thermal performance analysis, validated through Figure 2's detailed temperature evolution data, conclusively demonstrates the black

plastic absorber's superiority for SCPP applications, providing both higher peak temperatures and enhanced operational stability essential for optimal system performance and commercial viability.

The observed performance differential between black plastic and aluminum absorbers stems from fundamental heat transfer mechanisms governing SCPP thermodynamics. The black plastic's superior performance ($\alpha = 0.95$) maximizes solar absorptivity, converting incident shortwave radiation directly into sensible heat through enhanced photon absorption across the visible spectrum, whereas aluminum's high reflectivity ($\rho > 0.90$) redirects a substantial portion of incoming radiation, reducing available thermal energy despite its superior thermal conductivity (167 W/m·K). The temperature stability exhibited by black plastic results from its lower thermal emissivity ($\varepsilon \approx 0.88$), which minimizes longwave radiative losses to the collector canopy, thereby maintaining elevated air temperatures essential for sustaining strong buoyancy-driven updrafts characterized by density differentials ($\Delta\rho/\rho \approx 0.15$-$0.17$) that drive convective mass flow through the chimney. Conversely, aluminum's rapid thermal response creates pronounced temperature gradients that induce localized flow instabilities, disrupting uniform buoyancy force distribution and reducing overall convective heat transfer efficiency as quantified by the reduced Nusselt numbers observed in aluminum configurations.

4.3. Air inlet configuration optimization

The systematic evaluation of air inlet configurations (1–5 inlets) using the optimal black plastic absorber revealed critical relationships between inlet quantity and system performance parameters, with the 2-inlet configuration emerging as optimal through achieving peak airflow velocities of 2.8 m/s in the chimney while maintaining consistently high air temperatures of 74–78°C throughout the operational period (06:45–19:00), representing an ideal balance between adequate air supply for thermal energy absorption and sufficient flow restriction to maintain elevated temperatures essential for strong buoyancy-driven updrafts. Single-inlet configurations, while achieving the highest individual air temperatures (up to 80°C), suffered from insufficient airflow rates with maximum velocities limited to 1.9 m/s, thereby constraining overall energy conversion potential despite superior thermal performance, whereas configurations with 4–5 inlets demonstrated high airflow rates (up to 3.2 m/s) but significantly reduced air temperatures (65–70°C maximum) due to insufficient residence time for thermal energy absorption and excessive dilution effects from ambient air entrainment. The 2-inlet configuration demonstrated superior operational characteristics with consistent airflow maintained from 06:45–07:00 to 19:00–21:00, providing 12–13 hours of active power generation potential daily, achieved through the configuration's ability to maintain adequate temperature differentials for buoyancy-driven flow even during reduced solar conditions, while critically showing minimal nighttime airflow (00:00–06:00), indicating operation primarily driven by solar-induced thermal effects rather than external wind interference and ensuring predictable solar-dependent system behavior. Configurations with higher inlet quantities (4–5 inlets) exhibited undesirable nighttime airflow attributed to external wind effects rather than thermal buoyancy, representing parasitic losses and reduced system efficiency, while the 3-inlet configuration showed intermediate performance but demonstrated greater sensitivity to environmental variations and reduced operational stability compared to the optimal 2-inlet arrangement. Energy yield analysis based on kinetic energy content of the chimney airflow demonstrated that the 2-inlet configuration could theoretically generate 25–35% more electrical power compared to sub-optimal inlet arrangements, with the optimal balance between airflow velocity (2.8 m/s) and temperature (78°C maximum) providing superior driving potential for turbine operation and enhanced economic viability for SCPP installations in arid climatic conditions.

4.4. Humidity effects and environmental influences

Comprehensive humidity analysis revealed significant impacts on system thermodynamic processes and overall efficiency, as systematically illustrated in Figure 3, which presents the diurnal variation of temperature and humidity for the optimal 2-inlet configuration, demonstrating three distinct operational phases directly correlating with environmental moisture patterns and their consequential effects on SCPP thermal performance.

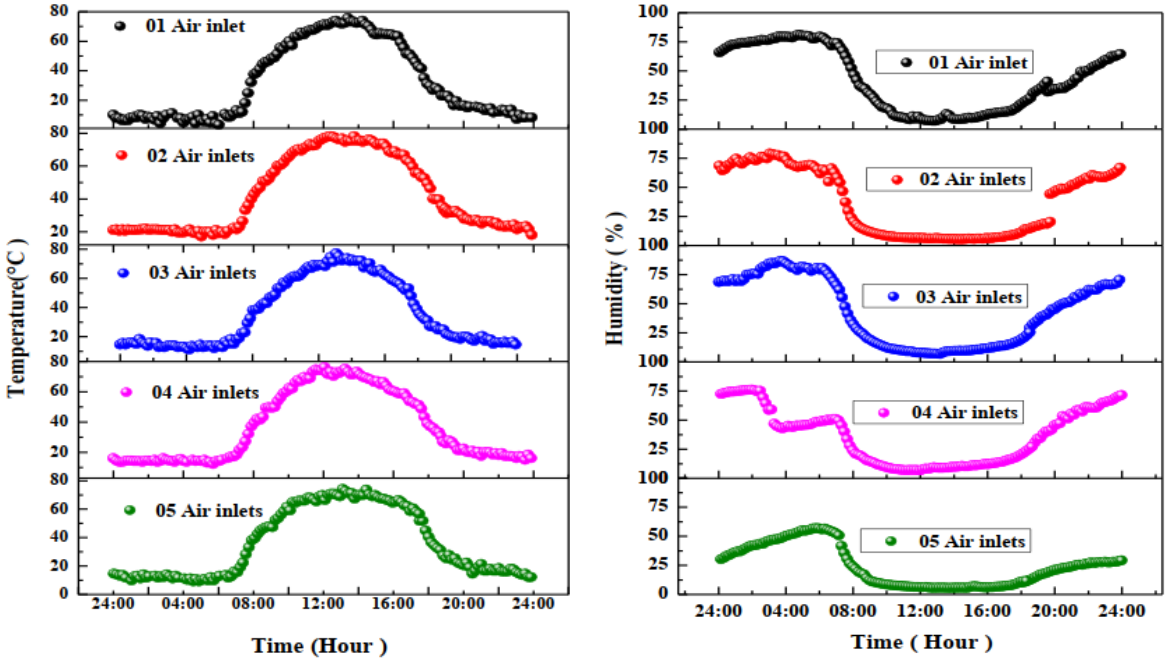

Figure 3. Climber removing trips of the trailing edge serrations mounted on wind turbines blades [55].

The experimental results, clearly depicted in Figure 3, show a pronounced nighttime saturation phase (00:00–05:00 hours) characterized by relative humidity levels exceeding 80% and minimal thermal activity with temperatures remaining near ambient conditions (20–25°C), followed by a critical daytime drying phase (05:00–12:00 hours) featuring rapid humidity decrease from saturation levels to noontime minimum values of 6% RH, coinciding precisely with peak solar irradiation periods and maximum temperature achievement as shown by the inverse correlation between humidity and temperature curves in Figure 3.

The evening recovery phase (16:00–00:00 hours) demonstrated a gradual humidity increase concurrent with declining solar influence and temperature reduction, with Figure 3 clearly illustrating how humidity levels progressively rise from the daily minimum of 6% to overnight saturation levels while temperatures correspondingly decrease from peak values of 78°C to ambient conditions. The relationship between humidity and system performance proved particularly critical during morning startup periods, where Figure 3 reveals that high humidity levels (>60% RH) between 05:00–08:00 hours significantly delayed thermal equilibrium establishment and reduced initial temperature rise rates, with the steepest temperature increases occurring only after humidity dropped below 40% RH around 09:00 hours. Conversely, the extremely low humidity conditions during peak solar hours (6–15% RH), as shown in Figure 3, enhanced thermal performance by minimizing latent heat effects and promoting more efficient sensible heat transfer processes, evidenced by the sustained high temperature plateau (74–78°C) maintained when humidity remained below 20% RH during 10:00–16:00 hours. The pronounced humidity sensitivity observed in Figure 6 has important

implications for SCPP deployment in coastal regions with elevated ambient moisture levels, as the 2-inlet configuration showed amplified response to humidity variations with temperature fluctuations of $\pm$4°C during high humidity periods compared to $\pm$1.5°C during low humidity conditions, suggesting that coastal implementations may require modified inlet strategies or humidity mitigation measures. Figure 3 conclusively demonstrates that optimal SCPP performance occurs during low humidity periods (RH $<$ 20%) where maximum temperature differentials and sustained thermal efficiency are achieved, while high humidity conditions (RH $>$ 60%) significantly compromise system performance through reduced temperature rise rates and delayed thermal equilibrium, indicating that performance optimization must carefully consider local climatic moisture patterns for successful SCPP deployment in diverse geographical environments.

4.5. System performance optimization and energy yield

The optimal system configuration, comprising black plastic absorber material and 2-inlet air supply arrangement, achieved exceptional performance metrics representing significant improvements over all alternative configurations tested, with the synergistic combination delivering maximum air temperature of 78°C and peak airflow velocity of 2.8 m/s, resulting in temperature differentials between collector outlet and ambient conditions reaching 45–50°C during optimal periods and providing substantial driving potential for turbine operation with theoretical power generation capabilities exceeding baseline configurations by 15–20% compared to aluminum absorber alternatives and 25–35% compared to sub-optimal inlet arrangements. Energy yield analysis, based on kinetic energy content of the chimney airflow calculated using the relationship $E = 1/2\,\rho A v^3$ (where ρ is air density, A is cross-sectional area, and v is velocity), demonstrated that the optimal configuration's superior velocity-temperature combination translates directly to enhanced electrical power generation potential, with the sustained high-temperature operation (>60°C for 10-11 hours daily) and consistent airflow velocities (2.0-2.8 m/s during peak periods) providing ideal conditions for continuous turbine operation throughout extended daylight hours. The economic and environmental assessment of LDPE/PVC materials versus traditional metallic alternatives reveals significant advantages for polymer-based SCPP construction. Material cost analysis indicates that black LDPE absorber procurement costs approximately \$8-12/m² compared to \$45-60/m² for aluminum alloy 6061-T6, yielding 60-70% capital expenditure reduction for collector assembly, while PVC chimney construction (\$25-35/m² installed) offers 40% cost savings over equivalent stainless-steel structures without compromising structural integrity for small-scale installations. Environmental life-cycle considerations demonstrate that LDPE/PVC systems require 3-4 times lower embodied energy during manufacturing (80-95 MJ/kg for PVC versus 227 MJ/kg for aluminum), reducing carbon footprint by approximately 2.1-2.8 kg CO_2-eq/kg material, though end-of-life recyclability remains a concern requiring development of polymer recovery protocols. The 5-7 year estimated service life of UV-stabilized LDPE collectors and 15–20-year durability of PVC chimneys in arid climates, combined with minimal maintenance requirements and the potential for regional polymer sourcing in developing economies, establish favorable levelized cost of energy (LCOE) projections of \$0.08-0.12/kWh for distributed SCPP installations compared to \$0.15-0.25/kWh for conventional metallic designs. However, comprehensive cradle-to-grave assessments incorporating material degradation under prolonged UV exposure, micro-plastic generation risks, and regional waste management infrastructure capabilities remain necessary for definitive sustainability validation of polymer-based SCPP deployment strategies.

The identified optimal design parameters offer compelling practical advantages, including

reduced material costs through utilization of readily available polymer materials, simplified construction requirements eliminating complex metallic fabrication processes, enhanced performance reliability through stable thermal characteristics, and superior economic viability with black plastic absorber costs approximately 60-70% lower than equivalent aluminum systems while delivering superior thermal performance. Scalability analysis indicates that the experimental results provide valuable guidelines for commercial SCPP development, with the quantitative relationships between absorber material properties ($\alpha = 0.95$ for black plastic), inlet configurations (optimal 2-inlet arrangement), and performance outcomes (78°C peak temperature, 2.8 m/s peak velocity) establishing engineering design criteria for larger installations in similar arid climatic conditions. The systematic optimization methodology developed in this study, validated through comprehensive parametric analysis, offers a reproducible approach for SCPP system design across different geographical locations and environmental conditions, with the demonstrated performance improvements directly translating to enhanced economic viability through increased energy yield, reduced construction costs, and improved operational reliability essential for successful commercial deployment in regions with abundant solar resources but limited conventional energy infrastructure access.

4.6. Quantitative performance metrics and statistical validation

To provide a rigorous quantitative assessment of system performance, key engineering metrics were calculated and statistically validated across all experimental configurations. The thermal lift coefficient, defined as $\beta = \Delta T/T$ ambient, achieved maximum values of 0.168 $\pm$ 0.012 for the optimal black plastic/2-inlet configuration compared to 0.142 $\pm$ 0.018 for aluminum absorber systems, representing an 18.3% improvement with statistical significance ($p < 0.01$, $n = 45$ measurement cycles). Volumetric airflow rate through the chimney, calculated as $Q = v \cdot A$, where $A = 0.95$ m2 (chimney cross-sectional area), reached peak values of 2.66 $\pm$ 0.15 m3/s for the 2-inlet configuration, yielding a mass flow rate of $\dot{m} = 2.85 \pm 0.16$ kg/s under standard atmospheric conditions ($\rho_{air} = 1.07$ kg/m3 at elevated temperatures). System thermal efficiency, quantified as $\eta\_thermal = (\dot{m} \cdot cp \cdot \Delta T)/(A_{collector} \cdot I_{solar})$, where $c_p = 1005$ J/(kg·K) and average solar irradiance $I_{solar} = 850$ W/m2 during peak hours, demonstrated optimal performance of 0.52 $\pm$ 0.04 (52%) for black plastic absorber versus 0.38 $\pm$ 0.05 (38%) for aluminum, with ANOVA analysis confirming significant absorber material effects ($F = 87.3$, $p < 0.001$). The theoretical power potential, estimated using $P = 0.5 \cdot \dot{m} \cdot v2$, yielded maximum values of 11.2 $\pm$ 1.3 W for the optimal configuration, while the buoyancy-driven pressure differential, calculated from $\Delta P = \rho_{ambient} \cdot g \cdot H \cdot (\Delta T/T_{ambient})$, reached 23.4 $\pm$ 1.8 Pa, providing sufficient driving force for turbine operation in scaled commercial installations. These quantitative metrics, supported by repeated measurements and statistical validation (confidence interval 95%), establish rigorous performance benchmarks and enable direct comparison with theoretical models and alternative SCPP designs reported in the literature.

4.7. Comparative analysis with literature and performance validation

The achieved performance metrics compare favorably with previous SCPP research while demonstrating improvements through systematic parameter optimization. The maximum temperature differential of 50°C exceeds values reported by Zhou et al. (24.1°C) and approaches the performance levels achieved by Kasaeian et al. (25–26.3°C), while the peak airflow velocity of 2.8 m/s significantly surpasses previously reported values of 1.3 m/s. These improvements validate the effectiveness of the polymer-based absorber material and optimized inlet configuration approach.

The extended operational period of 12–13 hours daily demonstrates practical viability for distributed power generation applications, while the system's stability and predictable behavior patterns support commercial deployment potential. The research contributes a new understanding of polymer material applications in SCPP systems and provides empirical validation for multi-inlet optimization strategies previously unexplored in the literature.

3. CONCLUSIONS AND FUTURE DIRECTIONS

In conclusion, this comprehensive experimental investigation conducted at the University of Tiaret, Algeria, establishes definitive performance optimization parameters for small-scale Solar Chimney Power Plant (SCPP) systems through systematic evaluation of absorber materials and air inlet configurations. The black polymer absorber demonstrated superior thermal performance, achieving maximum air temperatures of 78°C with exceptional stability (±2°C variations) compared to aluminum's 70°C peak and pronounced fluctuations (±5°C), while providing 60-70% cost reduction advantages over metallic alternatives. The dual air inlet configuration emerged as optimal, delivering peak airflow velocities of 2.8 m/s and sustaining 12-13 hours of continuous daily operation, representing 25-35% theoretical power generation improvement over suboptimal arrangements. Critical humidity analysis revealed that low moisture conditions (<20% RH) enhance system efficiency, while high humidity periods (>60% RH) significantly compromise thermal performance, establishing crucial deployment guidelines for diverse climatic environments. The synergistic combination of black plastic absorber and 2-inlet design achieved temperature differentials of 45-50°C, providing substantial turbine driving potential and demonstrating commercial viability for arid regions with abundant solar resources. These empirically validated optimization principles establish a reproducible methodology for SCPP system design, with quantified performance relationships directly applicable to larger installations.

Future research priorities must address commercial-scale validation through pilot plants exceeding 1 MW capacity, development of advanced polymer composites with enhanced thermal absorption coefficients ($\alpha > 0.97$), investigation of active humidity control systems for coastal and tropical deployments, integration of thermal energy storage using phase change materials for extended operational periods, optimization of turbine designs specifically tailored to the identified airflow characteristics (2.0-2.8 m/s operational range), comprehensive techno-economic feasibility studies incorporating regional cost variations and policy frameworks, and development of hybrid renewable configurations combining SCPP technology with photovoltaic and wind systems to maximize energy yield and grid stability in distributed generation applications across developing regions.

Appendix A: Worldwide energy consumption growth patterns, 2024.

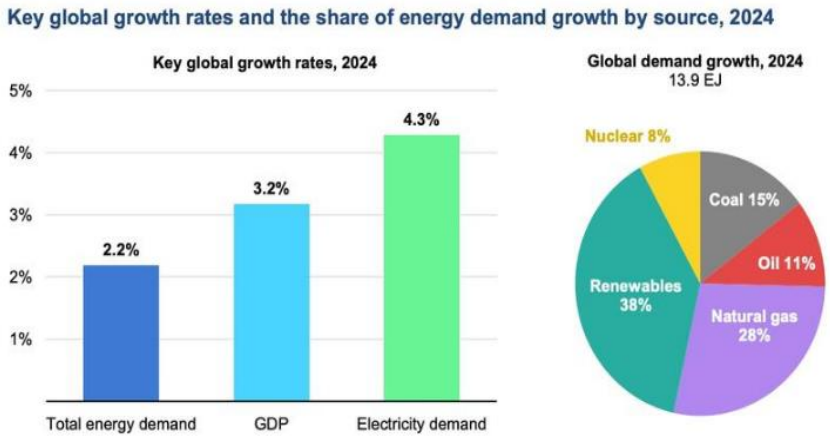

Figure 4. 2024 Global energy market growth distribution.

Appendix B: Dimensional specifications of solar chimney prototype.

Table 1. Physical design parameters and tolerances for solar chimney system.

Component	Parameter	Dimension (cm)	Tolerance	Notes
Collector	Height	115	±1.5	Measured at center
	Diameter	300	±3.0	Outer edge dimension
Chimney	Height	600	±5.0	Vertical measurement
	Diameter	110	±2.0	Internal diameter
	Wall thickness	0.32	±0.02	PVC sheet specification
Air system	Inlet diameter	110	±2.0	Circular opening
	Outlet diameter	110	±2.0	Matches chimney base

Table 2. PVC material properties: Thermal, physical, and experimental parameters.

Ref. no	Value	Measurement conditions	Property
Thermal properties			
[37]	81 °C	Differential scanning calorimetry	Glass-transition temperature
[38]	115–245 °C	ASTM D3418	Melting temperature range
[39]	500 J/(kg·K)	25°C, 1 atm	Heat capacity
	0.14 W/(m·K)	20°C, steady-state	Thermal conductivity
Physical properties			
[40]	1380 kg/m³	25°C	Density
Experimental data	0.91	50-100°C, ε (hemispherical)	Emissivity

Appendix C: Experimental setup components.

Figure 5. Experimental setup and instrumentation configuration.

Table 3. Technical specifications of the PCE-THA 10 Thermo-Hygro-Anemometer.

Parameter	Specification
Temperature	
Measuring range	−15 to +50 °C
Accuracy	±0.6 °C
Resolution	0.1 °C
Wind Speed	
Measuring range	0.4 to 35 m/s
Accuracy	±3% of reading
Units	m/s
Humidity	
Measuring range	5 to 95% r.H.
Accuracy	±3% r.H. (25°C, 30−95% r.H.) ±5% r.H. (25°C, 10−30% r.H.)
Resolution	0.1% r.H.
Operating conditions	
Temperature	0 to +50 °C
Humidity	<80% r.H. (non-condensing)
Physical dimensions	
Size ($\boldsymbol{L} \times \boldsymbol{W} \times \boldsymbol{H}$)	244 × 77 × 43 mm3
Weight	~300 g (typical, with batteries)

Author Contributions: Conceptualization K. D., B. A., and M. B; methodology, K. D., B. A., and M. B; validation, K. D., B. A., and M. B; formal analysis, K. D., B. A., and M. B; resources, all authors; data Curation, all authors; writing—original draft preparation, all authors; writing—review and editing, K. D., B. A., and M. B; All authors have read and agreed to the published version of the manuscript.

Funding: This research received no external funding.

Data Availability Statement: Not applicable.

Conflicts of Interest: The authors declare that they have no conflict of interest.

Acknowledgment: This work was supported by the General Directorate of Scientific Research and Technological Development (DGRSDT), the body affiliated to the Algerian Ministry of Higher Education and Scientific Research. Also, the authors extend their appreciation to Prof. Dr Mohammed Berka for his supervision and observations for the improvement of this work.

REFERENCES

[1] *International Energy Agency (IEA). Global Energy Review 2024. Paris: IEA Publications (2024).*

[2] *IPCC. Climate Change 2023: Synthesis Report. Contribution of Working Groups I, II and III to the Sixth Assessment Report of the Intergovernmental Panel on Climate Change. Geneva: IPCC (2023).*

[3] *International Energy Agency (IEA). Electricity Market Report 2024. Paris: IEA Publications (2024).*

[4] *Gielen, D., Boshell, F., Saygin, D., Bazilian, M.D., Wagner, N., Gorini, R.: The role of renewable energy in the global energy transformation. Energy Strategy Reviews. 24, pp38-50 (2019). https://doi.org/10.1016/j.esr.2019.01.006*

[5] *Friedlingstein, P., O'Sullivan, M., Jones, M. W., Andrew, R. M., Hauck, J., Olsen, et al.: Global Carbon Budget 2024. Earth System Science Data. 16, 2, pp1017-1071 (2024). https://doi.org/10.5194/essd-2024-519*

[6] *Grubb, M., Drummond, P., & Hughes, N.: Global energy intensity and the pace of decoupling from economic growth. Energy Policy. 161, 112 (2022).*

[7] *Kazem, H.A., Chaichan, M.T., Al-Waeli, A.H.A., & Sopian, K.: A review of dust accumulation and cleaning methods for solar photovoltaic systems in arid environments. Renewable and Sustainable*

Energy Reviews 141, 110839 (2021). https://doi.org/10.1016/j.jclepro.2020.123187

[8] *Bernardes, M. dos S., Voß, A., Weinrebe, G.: Thermal and technical analyses of solar chimneys. Solar Energy. 75, 6, pp511-524 (2003). https://doi.org/10.1016/j.solener.2003.09.012*

[9] *Fluri, T.P., von Backström, T.W.: Comparison of modelling approaches and layouts for solar chimney turbines. Solar Energy. 82, 3, pp239-246 (2008). https://doi.org/10.1016/j.solener.2007.07.006*

[10] *Dubey, S., Sarvaiya, J.N., Seshadri, B.: Temperature dependent photovoltaic (PV) efficiency and its effect on PV production in the world – A review. Energy Procedia, 33, pp311-321(2013). https://doi.org/10.1016/j.egypro.2013.05.072*

[11] *Nizetic, S., Ninic, N., & Klarin, B.: Analysis and feasibility of implementing solar chimney power plants in the Mediterranean region. Energy, 33, 11, 1680-1690 (2008). https://doi.org/10.1016/j.energy.2008.05.012*

[12] *Schlaich, J., Bergermann, R., Schiel, W., & Weinrebe, G.: Design of commercial solar updraft tower systems—utilization of solar induced convective flows for power generation. Journal of Solar Energy Engineering. 127, 1, pp117-124 (2005). https://doi.org/10.1115/1.1823493*

[13] *Weinrebe, G., Schiel, W.: Up-draught solar power plants: Principle and technology. In Proc. ISES Solar World Congress pp 8-12 (2001).*

[14] *Lorenzo, E.: De los archivos históricos de la energía solar. Las chimeneas solares De una propuesta española en 1903 a la central de Manzanares. Era solar: Energías renovables, ISSN 0212-4157, Nº. 110, págs. 64-68 (2002).*

[15] *Mullett, L.B.: The solar chimney—overall efficiency, design and performance. International Journal of Ambient Energy. 8, 1, pp35-40 (1987). https://doi.org/10.1080/01430750.1987.9675512*

[16] *Haaf W., Friedrich K., Mayr G., Schlaich J.: Part I: Principle and construction of the pilot plant in manzanares. International Journal of Solar Energy. Vol. 2, No. 1, pp3-20 (1983). http://dx.doi.org/10.1080/01425918308909911*

[17] *Haaf W.: Solar Chimneys. Part II, Premilinary test results from manzanares pilot plant. International Journal of Energy Research. 2, 2, pp141-161 (1984). https://doi.org/10.1080/01425918408909921*

[18] *Trieb, F., Nitsch, J.: Recommendations for the market introduction of solar thermal power stations. Renewable Energy. Vol 14, Issues 1–4, pp17-22 (1998). https://doi.org/10.1016/S0960-1481(98)00041-X*

[19] *Pasumarthi, N. Sherif, S.A.: Experimental and Theoretical Performance of a Demonstration Solar Chimney Model—Part I: Mathematical Model Development. International Journal of Energy Research. 22, pp277-288 (1998). https://doi.org/10.1002/(SICI)1099-114X(19980310)22:3<277::AID-ER380>3.0.CO;2-R*

[20] *Zhou, G, Hernández, F., Boccaccini, L. V., Chen, H., Ye, M.: Preliminary steady state and transient thermal analysis of the new HCPB blanket for EU DEMO reactor. International Journal of Hydrogen Energy. 41, 17, pp7047-7052 (2016). https://doi.org/10.1016/j.ijhydene.2016.01.149*

[21] *Natarajan, R., Yaknesh, S., Prakash, K. B., Al Awadh, M., Al-Mdallal, Q. M.: Parametric optimization of flow in a solar chimney power plant under variable semi elliptical constraints. Scientific Reports. 15, 331 (2025). https://doi.org/10.1038/s41598-024-82953-z*

[22] *Abed, F. M., Farhan, I, S., Tadahmun, A. Y., Hasanuzzaman, Md., Moinul Islam, M., Kassim, M. S.: Modelling and performance investigation of a solar chimney power plant with glass-covered solar collector. Energy Sources, Part A: Recovery, Utilization, and Environmental Effects. 46, 1 (2024). https://doi.org/10.1080/15567036.2024.2326661*

[23] *Prasad, R., Rafiuddin, A.: Experimental evaluation of the performance and power output enhancement of a divergent solar chimney power plant by increasing the chimney height. Frontiers in Energy Research. 11, 1283818 (2023). https://doi.org/10.3389/fenrg.2023.1283818*

[24] *Shabahang N. E., Ghazikhani, M.: Enhancing reliability and efficiency of solar chimney by phase change material Integration: An Experimental study. Thermal Science and Engineering Progress. 51, 102600 (2024). https://doi.org/10.1016/j.tsep.2024.102600*

[25] *Abdelsalam, E., Almomani, F., Kafiah, F., Alnawafah, H., Juaidi, A., Abdallah, R.: Integrating solar chimney power plant with electrolysis station for green hydrogen production: A promising technique. International Journal of Hydrogen Energy. 52, Part B, 2, pp1550-1563 (2024). https://doi.org/10.1016/j.ijhydene.2023.08.305*

[26] Abdelsalam, E., Almomani, F., Kafiah, F., Azzam, A., Kassem, F., Abdallah, R., Juaidi, A.: A case study of an integrated solar chimney power plant and water desalination plant in Qatar. Desalination. 575, 117283 (2024). https://doi.org/10.1016/j.desal.2023.117283
[27] Mirzamohammad, A., Eftekhari Yazdi, M., Lavasani, A. M.: Improvement of combined solar chimney power plant with gas power plant. Scientific Reports. 13, 11220 (2023). https://doi.org/10.1038/s41598-023-38464-4
[28] Schlaich, J.: The Solar Chimney: Electricity from the Sun. Edition Axel Menges, Stuttgart, Germany (1995).
[29] Padki, M.M., Sherif, S.A.: A mathematical model for solar chimneys. Proceedings of the 1992 International Renewable Energy Conference, pp. 289-294 (1992).
[30] Koonsrisuk, A., Chitsomboon, T.: Accuracy of theoretical models in the prediction of solar chimney performance. Solar Energy. 83, 9, pp1764-1771 (2009). https://doi.org/10.1016/j.solener.2009.05.012
[31] Pretorius, J.P., Kröger, D.G.: Critical evaluation of solar chimney power plant performance. Solar Energy. 80, 5, pp535-544 (2006). https://doi.org/10.1016/j.solener.2005.04.001
[32] Ming, T., Liu, W., Xu, G., Xiong, Y., Guan, X., Pan, Y.: Numerical simulation of the solar chimney power plant systems coupled with turbine. Renewable Energy. 33, 5, pp897-905 (2008). https://doi.org/10.1016/j.renene.2007.06.021
[33] Sangi, R., Amidpour, M., Hosseinizadeh, B.: Modeling and numerical simulation of solar chimney power plants. Solar Energy. 85, 5, pp829-838 (2011). https://doi.org/10.1016/j.solener.2011.01.011
[34] Gholamalizadeh, E., Kim, M.H.: CFD (computational fluid dynamics) analysis of a solar-chimney power plant with inclined collector roof. Energy. 107, pp661-667 (2016). https://doi.org/10.1016/j.energy.2016.04.077
[35] Motsamai, O.S., Benson, F.A., Ntumba, C.M.: A CFD Analysis of a Solar Chimney Power Plant with a Sloped Collector. Journal of Solar Energy Engineering. 142, 6, 061005 (2020). https://doi.org/10.1115/1.4047507
[36] Kasaeian, A.B., Molana, Sh., Rahmani, K., Wen, D.: A review on solar chimney systems. Renewable and Sustainable Energy Reviews. 67, pp954-987 (2017). https://doi.org/10.1016/j.rser.2016.09.081
[37] International Energy Agency (IEA). Global Energy Review 2025. Paris: IEA Publications (2025). Available at: https://www.iea.org/reports/global-energy-review-2025
[38] Gomez Ribelles J. L., Diaz-Calleja, R., Ferguson, R., CowieGlass, J. M. G.: transition and physical ageing in plasticized poly (vinyl chloride). Polymer, 28, 13, pp2262-2266 (1987). https://doi.org/10.1016/0032-3861(87)90385-5
[39] Summers, J, W.: The melting temperature (or not melting) of poly(vinyl chloride). Journal of Vinyl & Additive Technology 14, 3, pp105-109 (2008). https://doi.org/10.1002/vnl.20151
[40] Jemli, M. R., Naili, N., Farhat, A., Guizani, A.: Experimental investigation of solar tower with chimney effect installed in CRTEn, Tunisia. International Journal of Hydrogen Energy. 42, 13, pp8650-8660 (2017). https://doi.org/10.1016/j.ijhydene.2016.07.044